International Journal of Dynamics and Control (2022) 10:1021–1033
https://doi.org/10.1007/s40435-021-00883-4

Local bifurcation of brushless DC motor through a mechanical parameter: the viscous damping coefficient

Philippe Byaombe Faradja[1,2] · Guoyuan Qi[3] · Fabrice M. Kabonzo[4]

Received: 5 May 2021 / Revised: 7 October 2021 / Accepted: 8 October 2021 / Published online: 11 November 2021

Abstract

The dynamics of brushless DC motor (BLDCM) is studied in detail from the viscous damping coefficient, a mechanical parameter. While this parameter intervenes in determining the dissipativity of the system; it shows the high complexity of the brushless DC motor. The pitchfork bifurcation is revealed. The Hopf bifurcation is identified twice in the road towards and from chaotic dynamics regions. Rigorous methods such as the center manifold theorem and the normal form theory confirm Hopf bifurcation. The different theoretical scenarios and motor parameters are also illustrated. Real positive parameters of the coefficient are only considered to keep the physical meaning from the analysis. With some special conditions around Hopf bifurcation, the transient chaotic behaviors of the BLDCM are detected. Bifurcation diagrams and Lyapunov exponents are used to support the theoretical findings.

Keywords BLDCM · Damping coefficient · Local bifurcation · Chaos · Hopf bifurcation · Nonlinear systems

1 Introduction

Various electromechanical systems such as dynamo [1], driven double pendulum [2], driven triple pendulum [3], inverted pendulum [4], beam coupled with an oscillator [5], and electromechanical transducer [6] have attracted focus due to their interesting dynamics. However, the brushless DC motor (BLDCM) has been of the most studied electromechanical systems. Especially relating to chaos theory, Hemati studied the equilibria and dynamic characteristics (chaos) of a class of motors from their compact form [7]. Similar to the BLDCM model, the synchronous reluctance motor drive (SynRM) model exhibited Hopf bifurcation via one of its input [8].

✉ Philippe Byaombe Faradja
bfaradja@gmail.com

1 School of Electrical Engineering, Academy of Science and Technology (ASCITECH), Ngaliema, Kananga 44, Kinshasa, Democratic Republic of Congo

2 Software and Hardware Design (SHD) Africa, Bandal-Paris, Tonde 186, Kinshasa, Democratic Republic of Congo

3 Tianjin Key Laboratory of Advanced Technology of Electrical Engineering and Energy, Tiangong University, Tianjin 300387, People's Republic of China

4 School of Electrical and Information Engineering, Tianjin University, Tianjin 300072, People's Republic of China

Hemati has non-dimensionalized the BLDCM [9]. In most studies, the BLDCM model has been non-dimensionalized [10] since it possesses many parameters. While the aim was to make the analysis easier, the richness of the dynamics was hidden. As a result, the BLDCM has been often compared to the Lorenz system [9]. In real life, this comparison has not been useful due to bifurcation in the real system design.

For reference, the BLDCM or the general permanent magnet synchronous motor (PMSM) has also been studied in terms of control with linear control feedback [11], global control [12], dynamic surface control [13].

Furthermore, for synchronization, single-variable coupling [14], various coupling terms and linearization of error dynamics [15], the backstepping design, and the Gerschgorin's theorem method [16] were used.

The bifurcation analysis for these models of BLDCM, including both fractional-order [17] and integer-order [18, 19] have been conducted; however, the methods like Lyapunov exponents or bifurcation diagram are non-rigorous.

Besides the self-excited chaos, the hidden chaos was investigated. The hidden chaos was first reported in the original BLDCM [20, 21] and then in the modified model of PMSM.

The hidden chaos has proven dangerous in multistability in the BLDCM as investigated by Faradja and Qi [21] and adopted for plasma system study by Yang et al. [22] and unmanned aerial vehicles by Bi et al. [23].

Besides traditional bifurcation techniques, other mechanisms to explain dynamics in the BLDCM were investigated, like energy-based methods using Casimir functions and Kolmogorov systems [24], using generalized Hamiltonian functions explained the onset of different dynamical behaviors such as sink, limit cycle, chaos [25].

While traditional bifurcation studies use non-dimensionalized models and energy-based methods refer more to force and energy, the studies on the dynamics of BLDCM, however, are still lacking some insight. Studies of the effects of individual parameters of BLDCM have not been conducted in general. A few exceptional studies exist. Gao systematically studied the permanent-magnet sizing effect [26], compared in that study with the motor torque constant with the same dimension as the permanent magnet flux. Recently, Faradja and Qi considered the bifurcation with the direct-axis voltage as the bifurcation parameter [27]. The BLDCM possesses design parameters such as the viscous damping coefficient (Table 1).

To the best of our knowledge, bifurcation of the BLDCM with the viscous damping parameter has not been analyzed. It should be considered that the non-dimensionalization has introduced other problems. For example, it is impossible to obtain chaos with a real motor with the chosen parameters because some real parameters will be abnormally negative, as illustrated by Li et al. [10] and Singh et al. [28].

The paper's main finding is that the bifurcation contribution of the damping coefficient in the overall system dynamics is highly complex, even in a real context. Both non-rigorous and rigorous methods are used.

The paper is organized as follows. The model of the BLDCM is described in Sect. 2. The bifurcation analysis exposing the pitchfork and Hopf bifurcation are detailed in Sect. 3. Section 4 deals with the illustration of the different scenarios of bifurcation. The paper is concluded in Sect. 5.

Table 1 Categorization of literature on dynamics of PMSM/BLDCM

Category of papers	Sub-classification/remarks	References of papers
Chaos and Dynamics from non-dimensionalized models	Reduce the design complexity	[7, 9]
Control and synchronization of BLDC/PMSM	Control (linear and nonlinear methods, local and global approach	[11–13]
	Synchronization	[14–16]
Bifurcation analysis	With non-rigorous methods	[7, 9, 10, 17–19]
Hidden chaos in BLDCM/PMSM	Transient hidden chaos in the normal BLDCM/PMSM model	[20, 21]
	Input excited via feedback in a problematic modified BLDCM/PMSM model	[28]
Dynamics with energy based methods	Using Casimir energy function from Kolmogorov systems	[24]
	Using Hamiltonian function	[25]
Dynamics with singular parameter	Electromechanical parameter: motor torque constant	[26]
	Electrical input: Direct axis voltage	[27]
	Mechanical design parameter: damping coefficient	This paper

2 Model description of BLDCM

The non-salient-pole (or smooth air gap) BLDCM model in the rotating frame (d-q) obtained after a Park transformation comprises differential equations for three state variables [9] is expressed as follows:

$$\begin{aligned}\frac{di_q}{dt} &= \left(-Ri_q - nL\omega i_d - nk_t\omega + v_q\right)/L,\\ \frac{di_d}{dt} &= \left(-Ri_d + nL\omega i_q + v_d\right)/L,\\ \frac{d\omega}{dt} &= \left(nk_t i_q - b\omega - T_L\right)/J,\end{aligned} \tag{1}$$

where i_q the quadrature-axis current, i_d the direct-axis current, ω rotor velocity; t is the elapsed time; for the parameters, R is the winding resistance matrix with $L = \frac{3}{2}L_a$, L_a the self-inductance of the winding, n the number of permanent-magnet pole pairs, $k_t = \sqrt{3/2}k_e$, k_e the coefficient of motor torque, J the moment of inertia, b the damping coefficient; for the input variables, v_q and v_d are the voltages across the quadrature axis and direct axis, respectively, and T_L the external torque. This model describes a smooth air-gap machine where the variation of reluctance in the air gap L_g is zero.

The following assumptions are made: $v_q = 0$ and $T_L = 0$.

The divergence of the BLDCM model is $\nabla V = -(2R/L + b/J)$, so the system is dissipative when all parameters have sound meanings under the condition $\nabla V < 0$.

Hence, the volume in phase space shrinks exponentially to zero. Also, the energy of the system will become nulled with the absence of inputs. The existence of the damping coefficient in the gradient shows the importance of this parameter.

3 Bifurcation analysis with damping coefficient

We now consider the viscous damping coefficient as the bifurcation parameter. The equilibrium number changes with parametric conditions under the stated assumptions. With the assumptions stated above, the equilibria are obtained. Settingthen the three equilibria are

$$\begin{aligned}&-Ri_q - nL\omega i_d - nk_t\omega = 0,\\&-Ri_d + nL\omega i_q + v_d = 0, \text{ and } nk_t i_q - b\omega = 0,\end{aligned}$$

$$\begin{aligned}&E_1 = \left[0, \frac{v_d}{R}, 0\right],\\&E_{2,3} = \left[\pm\frac{1}{n^2k_tL}\sqrt{\Delta},\ -\frac{bR + k_t^2n^2}{k_tLn^2},\ \pm\frac{1}{nbL}\sqrt{\Delta}\right]\end{aligned} \tag{2}$$

where

$\Delta = -bR^2(b - b_p)$ and $b_p = -\left(k_t^2n^2R + k_tv_dLn^2\right)\Big/R^2.$

Therefore, the BLDCM undergoes pitchfork bifurcation when the damping coefficient takes the value

$$b_p = -\left(k_t^2n^2R + k_tv_dLn^2\right)\Big/R^2. \tag{3}$$

At this value, the number of equilibrium points changes from three for $b < b_p$ to one for $b > b_p$. The occurrence of pitchfork bifurcation is thus observed. The first equilibrium can be saddle-node or sink except when its stability cannot be determined by eigenvalues rather by the center manifold theorem. The equilibria are also found in [27].

For the other equilibria, the characteristic polynomial is written as

$$P(\lambda) = \lambda^3 + \frac{2JR + bL}{JL}\lambda^2 + \frac{-Jk_t^2Rn^2 - Jk_tLn^2v_d + LRb^2}{JL^2b}\lambda - \frac{2k_t^2n^2R + 2k_tv_dLn^2 + 2bR^2}{JL^2} \tag{4}$$

The study of the stability of this characteristic polynomial requires that

$$\frac{2JR + bL}{JL} > 0, \tag{5}$$

meaning that $2JR + bL > 0$. Then we also have

$$\frac{-Jk_t^2Rn^2 - Jk_tLn^2v_d + LRb^2}{JL^2b} > 0. \tag{6}$$

And finally,

$$-\frac{2k_t^2n^2R + 2k_tv_dLn^2 + 2bR^2}{JL^2} > 0. \tag{7}$$

Based on these three conditions, we have

$$b < b_P \tag{8}$$

with

$$b_p = -\left(k_t^2n^2R + k_tv_dLn^2\right)\Big/R^2$$

The condition of Eq. (8) relates the stability of the symmetric equilibria to pitchfork bifurcation. This value b_P is the critical value for the occurrence of pitchfork bifurcation. Inequalities (7) and (8) are necessary conditions for the stability of the symmetric equilibria.

The sufficient condition is drawn from the Routh-Hurwitz table. If the characteristic polynomial in Eq. (4) is $s^3 + As^2 + Bs + C = 0$, the sufficient condition is $(AB - C)/A > 0$. Hence,

$$\frac{-2J^2k_t^2R^2n^2 - 2v_dJ^2k_tLRn^2 + Jk_t^2LRbn^2 + v_dJKL^2bn^2 + 4JLR^2b^2 + L^2Rb^3}{2JLb\left(k_t^2Rn^2 + Lv_dk_tn^2 + bR^2\right)} > 0. \tag{9}$$

This inequality is essential. Considering the real case scenario with positive parameters, this inequality shows complexity with the bifurcation using the mechanical parameter. Pravin analyzed the possibility of obtaining real roots from cubic equations [29].

For Hopf bifurcation, three conditions are needed: (1) nonhyperbolicity, (2) transversality condition, and (3) nongenericity.

For the first condition of nonhyperbolicity, it is supposed from Eq. (9) that there is an eigenvalue $\lambda = \theta j$, then the critical value is obtained from

$$\frac{-2J^2k_t^2R^2n^2-2v_dJ^2k_tLRn^2+Jk_t^2LRbn^2+v_dJKL^2bn^2+4JLR^2b^2+L^2Rb^3}{2JLb\left(k_t^2Rn^2+Lv_dk_tn^2+bR^2\right)} = 0. \tag{10}$$

Equation (10) possesses three roots:

$$b_{H0} = -\frac{b_{dc1}}{2} - \frac{b_{dc2}}{2b_{dc1}} - \frac{4JR}{3L} - \sqrt{3}\left(\frac{b_{dc2}}{2b_{dc1}} - \frac{b_{dc1}}{2}\right)j, \tag{11a}$$

$$b_{H1} = -\frac{b_{dc1}}{2} - \frac{b_{dc2}}{2b_{dc1}} - \frac{4JR}{3L} + \sqrt{3}\left(\frac{b_{dc2}}{2b_{dc1}} - \frac{b_{dc1}}{2}\right)j, \tag{11b}$$

$$b_{H2} = b_{dc1} + \frac{b_{dc2}}{b_{dc1}} - \frac{4JR}{3L}, \tag{11c}$$

with

$$b_{dc1} = \sqrt[3]{\left[\sqrt{\left(b_{dc4} - \frac{64J^3R^3}{27L^3} + b_{dc3}\right)^2 - b_{dc2}^3}\right] + b_{dc4} - \frac{64J^3R^3}{27L^3} + b_{dc3}},$$

$$b_{dc2} = \frac{16J^2R^2}{9L^2} - \frac{b_{dc5}}{R},\ b_{dc3} = \frac{2J^2k_t^2R^2n^2 + 2Lv_dJ^2k_tRn^2}{2L^2R},$$

$$b_{dc4} = 2Jb_{dc5},\ b_{dc5} = \frac{JRk_t^2Ln^2 + Jv_dk_tL^2n^2}{3L^2}.$$

By solving the corresponding equation with respect to v_d, we get

$$v_{d1} = -\frac{k_tR}{L}, \tag{14a}$$

$$v_{d2} = -\frac{R\left(59JR^2 + 2k_t^2Ln^2 + 11\sqrt{33}JR^2\right)}{2k_tL^2n^2}, \tag{14b}$$

$$v_{d3} = -\frac{R\left(59JR^2 + 2k_t^2Ln^2 - 11\sqrt{33}JR^2\right)}{2k_tL^2n^2} \tag{14c}$$

The second condition (14b) implies that

The analysis of the stability with complex roots must consider the real case scenario. The three roots in Eq. (11) are real for specific conditions. According to Pravin [29], if the numerator of the polynomial in Eq. (10) is written as

$$b^3 + B_2b^2 + B_1b + B_0,$$

then the three roots are real when the following conditions are fulfilled

$$\left(2B_2^3 - 9B_2B_1 + 27B_0\right)^2 \leq 4\left(B_2^2 - 3B_1\right), \tag{12a}$$

$$\left(B_2^2 - 3B_1\right) \geq 0. \tag{12b}$$

For the first condition (12a), we obtain

$$\frac{108J^3k_t^6}{L^3} + \frac{6372J^4k_t^4R^2n^4}{L^4} - \frac{13824J^5k_t^2R^4n^2}{L^5} + \frac{6372J^4k_t^2v_d^2n^4}{L^2} + \frac{108J^3k_t^3v_d^3n^6}{R^3} + \frac{324J^3k_t^5v_dn^6}{L^2R} + \frac{324J^3k_t^4v_d^2n^6}{LR^2} + \frac{12744J^4k_t^3Rv_dn^4}{L^3} - \frac{13824J^5k_tR^3v_dn^2}{L^4} \leq 0. \tag{13}$$

$$\frac{16J^2R^2}{L^2} - \frac{3Jk_t^2n^2}{L} - \frac{3Jk_tv_dn^2}{R} \geq 0, \tag{15}$$

so that $v_d \leq v_{d4}$ with

$$v_{d4} = \left(-3Lk_t^2Rn^2 + 16JR^3\right)\Big/3k_tL^2n^2. \tag{16}$$

It is straightforward to observe that $v_{d2} < v_{d1}$, $v_{d3} > v_{d1}$ and $v_{d1} < v_{d4}$. Therefore the polynomial possesses three roots when

$$v_d \leq v_{d2}. \tag{17}$$

When the number of pole pairs is extremely high,

$$v_{d_4} = -k_tR/L. \tag{18}$$

We now test the second condition, i.e., the transversality condition. We recall the characteristic polynomial again in another format

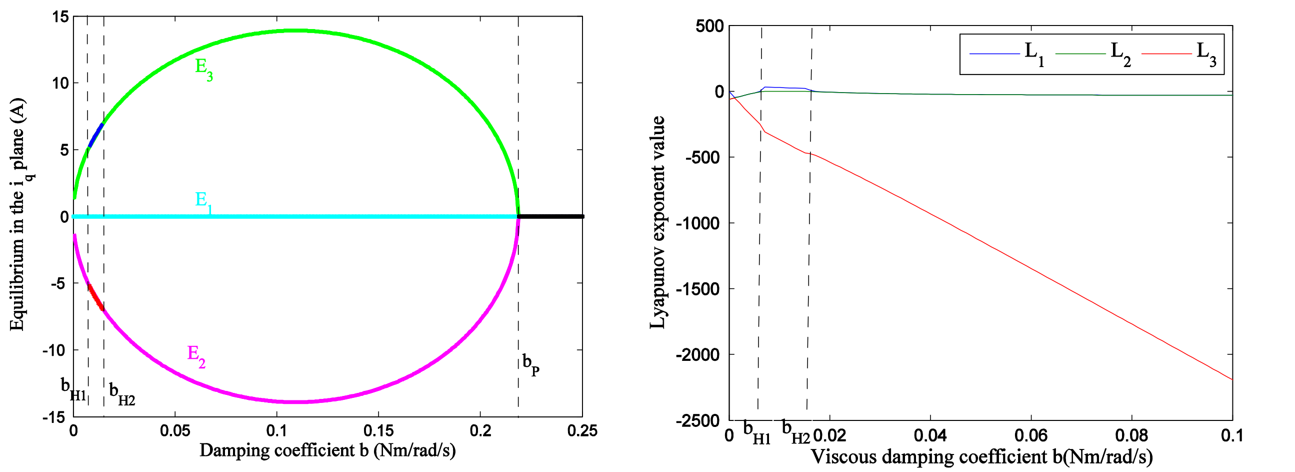

(a) stability of the different equilibria (b) Lyapunov spectrum, $\left[i_q(0), i_d(0), \omega(0)\right] = [0.2, 0.1, 0.1]$

Fig. 1 Evolution of dynamical behaviors (Color figure online)

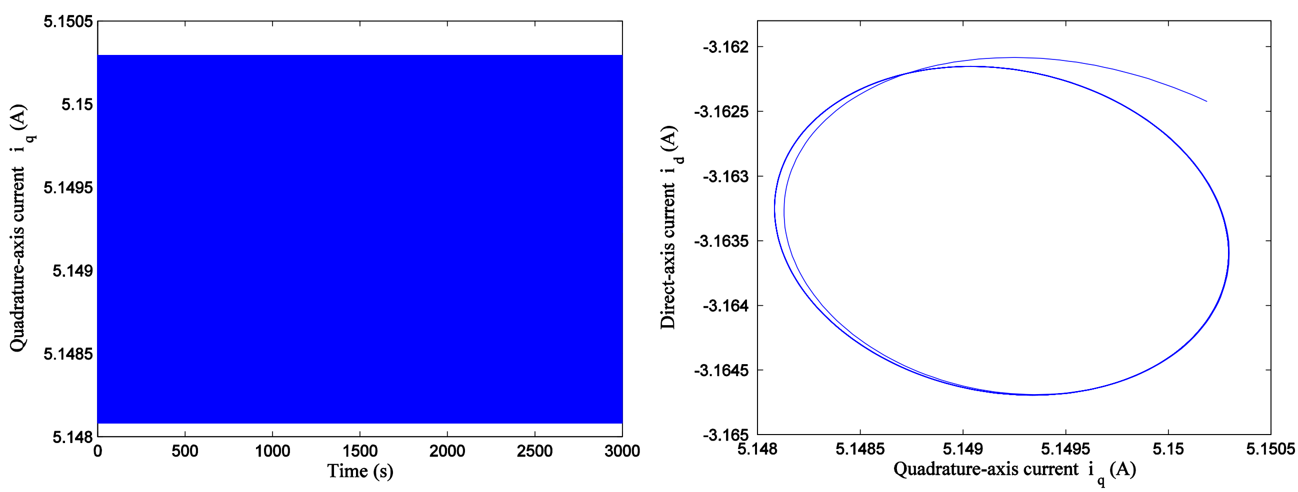

(a) Time series of limit cycle (b) phase trajectory of limit cycle

Fig. 2 Limit cycle of Hopf bifurcation

$$P(\lambda) = \lambda^3 + \frac{2JLR + bL^2}{JL^2}\lambda^2 + \frac{LRb^2 - Jk_t^2Rn^2 - Jk_tLn^2k_tv_d}{JL^2b}\lambda - \frac{2k_t^2n^2R + 2k_tv_dLn^2 + 2bR^2}{JL^2}. \tag{19}$$

The polynomial is thus derived for the damping coefficient with the eigenvalue being a function of the same parameter,

$$3\lambda^2 d\lambda + 2\frac{2JLR + bL^2}{JL^2}\lambda d\lambda + \frac{-Jk_t^2Rn^2 - Jk_tLn^2k_tv_d + LRb^2}{JL^2b}d\lambda + \frac{\lambda^2}{J}db - \frac{2R^2}{JL^2}db + \frac{R\lambda}{JL}db + \frac{Jk_t^2Rn^2 + Jk_tLn^2v_d}{JL^2b^2}\lambda db. \tag{20}$$

Extracting the ratio of change of the eigenvalue with respect to the bifurcation parameter, and using the conjugate of the complex denominator yield

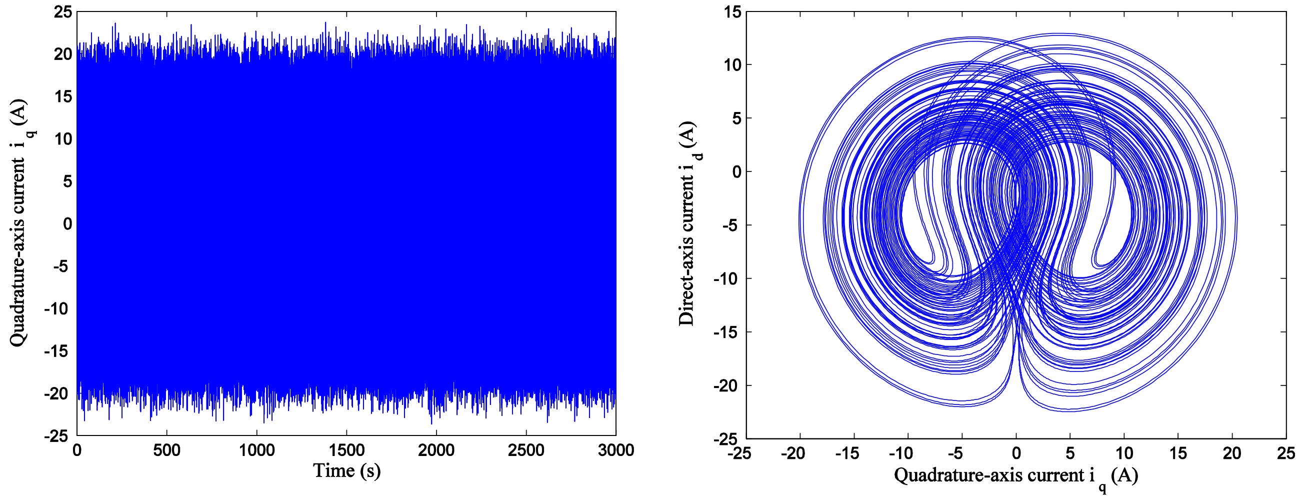

(a) Time series of non-Shilnikov chaos (b) phase trajectory of non-Shilnikov chaos

Fig. 3 Non-Shilnikov self-excited chaos

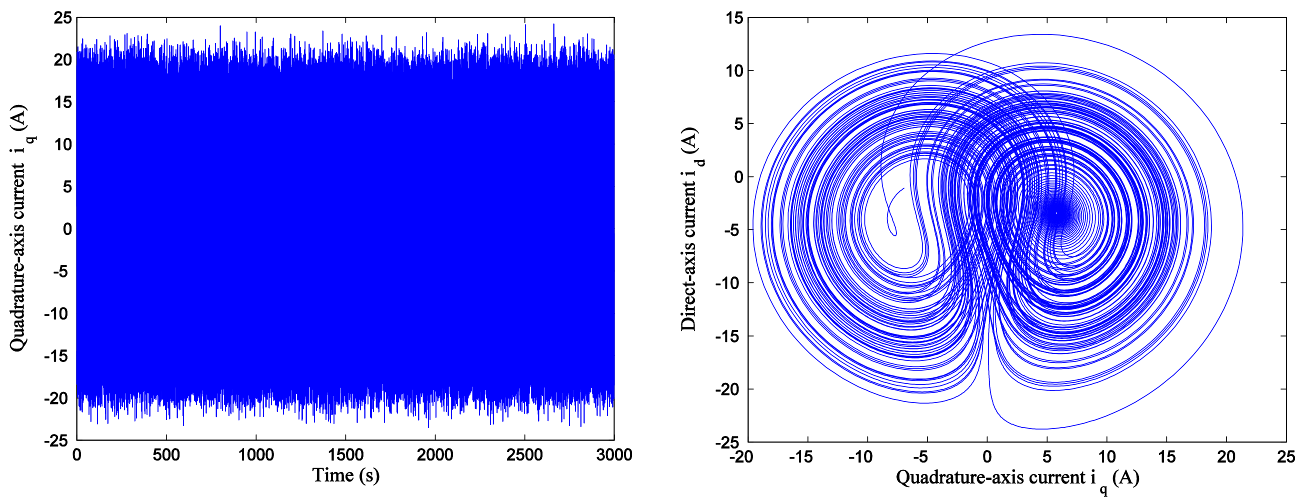

(a) Time series of self-excited chaos (b) phase trajectory of self-excited chaos

Fig. 4 Shilnikov self-excited chaos

$$\frac{d\lambda}{db} = -\frac{\left(-\frac{\theta^2}{J} - \frac{2R^2}{JL^2} + \frac{R\theta j}{JL} + \frac{Jk_t^2Rn^2 + Jk_tLn^2v_d}{JL^2b^2}\theta j\right)\left(-2\theta^2 - 2\frac{2JLR+bL^2}{JL^2}\theta j\right)}{\left(-2\theta^2 + 2\frac{2JLR+bL^2}{JL^2}\theta j\right)\left(-2\theta^2 - 2\frac{2JLR+bL^2}{JL^2}\theta j\right)}. \tag{21}$$

The real part of the change of the eigenvalue becomes

$$\mathrm{Re}\left(\frac{d\lambda}{db}\right) = \frac{2J^2k_t^2R^2n^2 + 2v_dJ^2k_tLRn^2 + Jk_t^2LRbn^2 + v_dJk_tL^2bn^2 + JL^3b^2\theta^2 + 4JLR^2b^2 + L^2Rb^3}{2\theta^2 + 2\left(\frac{2JLR+bL^2}{JL^2}\right)^2}. \tag{22}$$

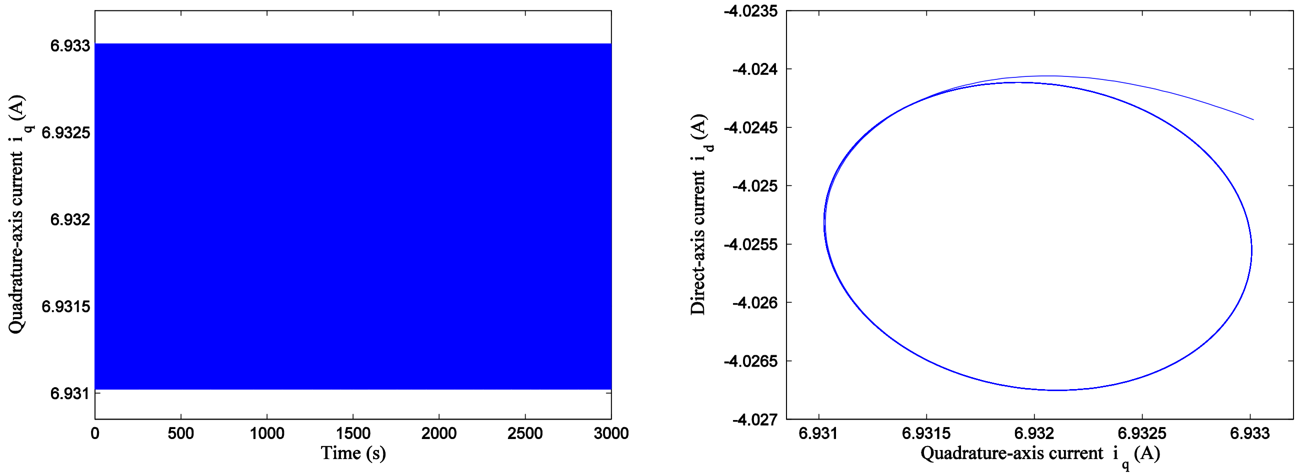

(a) Time series of limit cycle (b) phase trajectory of limit cycle

Fig. 5 Limit cycle of Hopf bifurcation

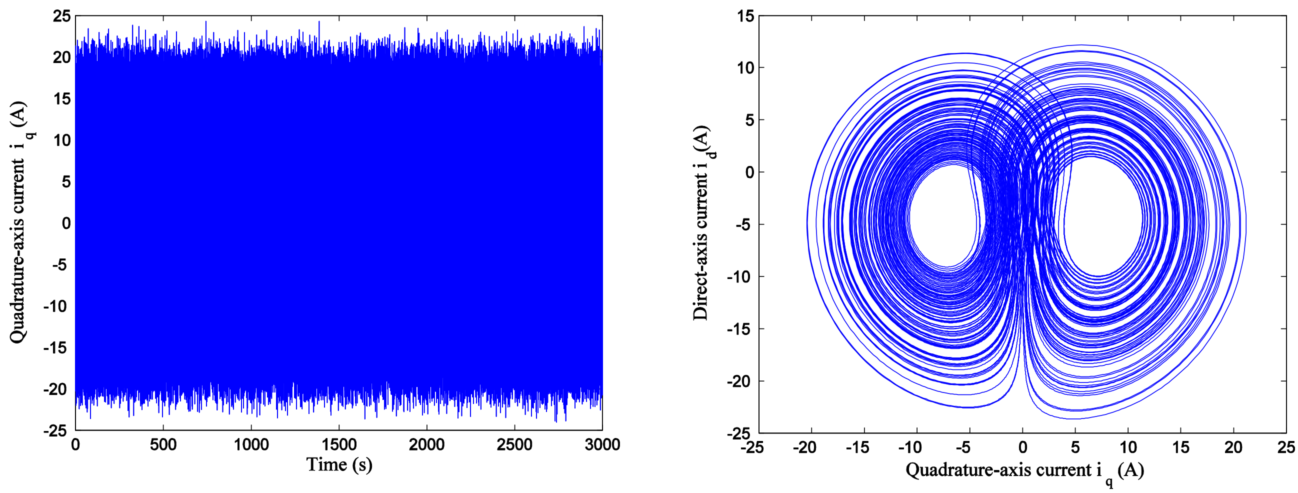

(a) Time series of self-excited chaos (b) phase trajectory of self-excited chaos

Fig. 6 Non-Shilnikov self-excited chaos

The transversality condition is fulfilled when

$$\mathrm{Re}\left(\frac{d\lambda}{db}\right) \neq 0, \tag{23}$$

which means

$$v_d \neq -\frac{J^2k_t^2Rn^2 + 2RJLb^2 + L^2b^3}{J^2k_tLn^2}, \tag{24a}$$

$$R \neq 0, \tag{24b}$$

$$R \neq -\frac{J^2k_tLn^2v_d + L^2b^3}{J^2k_t^2n^2 + 2JLb^2}. \tag{24c}$$

Remark 1 This value $v_d = v_{d2}$ from Eq. (14b) is significant for two-dimensional bifurcation combining v_d and b as it determines the critical value beyond which there is no Hopf bifurcation. In fact, at this value $b_{H1} = b_{H2}$, Hopf bifurcation may exist without chaos. This value also has an impact on transient chaos. It determines the critical value of transient chaos.

By increasing or decreasing the value, the duration of transient chaos decreases. So it becomes the single point where permanent chaos occurs. We have thus the single-value permanent chaos. Chaos occurs only at those parameter values in the 2D plane. At the values $b = b_{H1}$ [Eq. (11b)] and $b = b_{H2}$ [Eq. (11c)], the non-hyperbolicity condition is satisfied.

The third condition, i.e., non-genericity, of the Hopf bifurcation can be applied through the center manifold theorem with the viscous damping coefficient. For these two positive points $b = b_{H1}$ [Eq. (11b)] and $b = b_{H2}$ [Eq. (11c)],

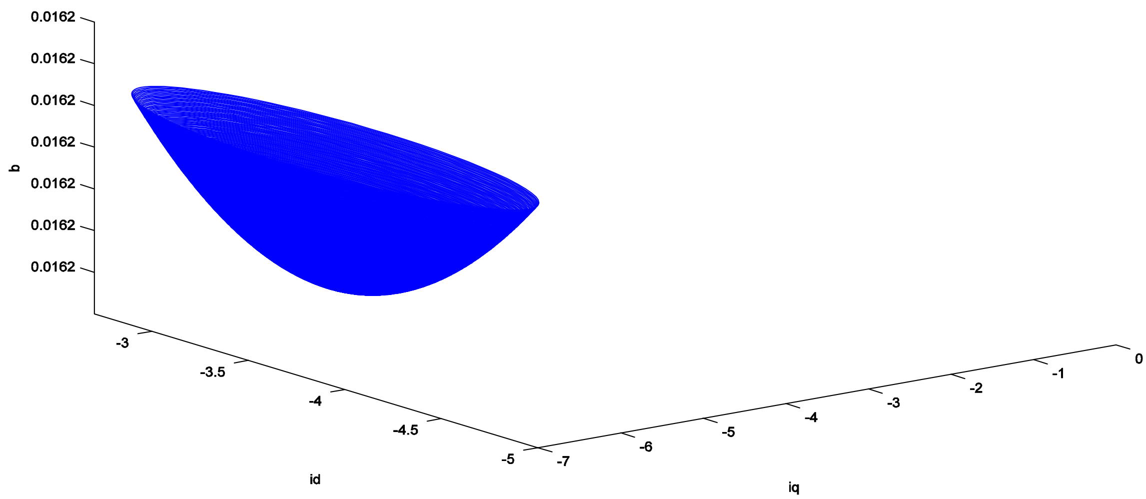

Fig. 7. 3D family of limit cycles

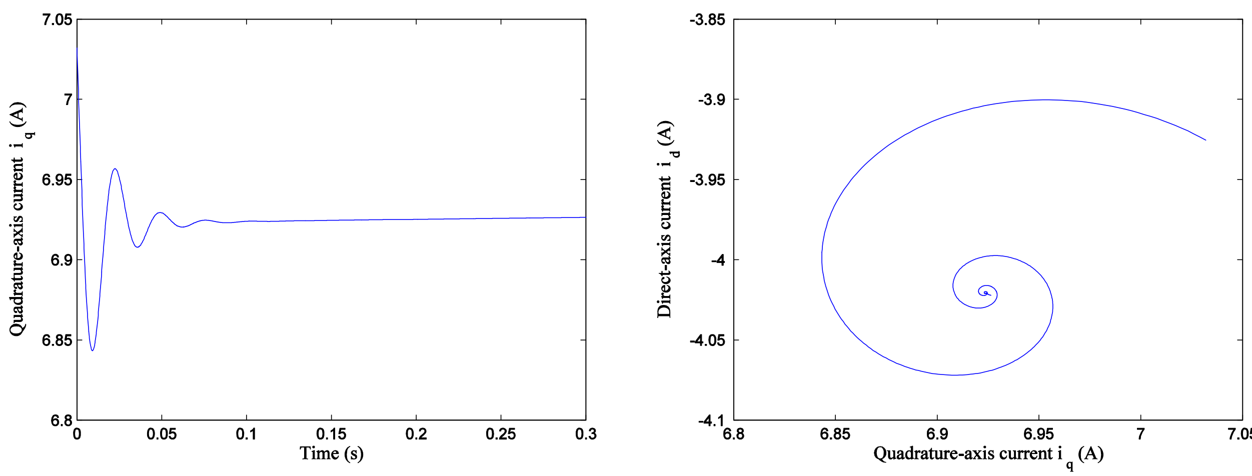

(a) Time series for an exception

(b) Phase trajectory for an exception

Fig. 8 Special case for the parameters

we apply the center manifold theorem and the normal form theory developed by Faradja and Qi [27] to obtain non-zero first Lyapunov coefficients at both values. We have supercritical Hopf bifurcation at both points. Equilibria E_2 and E_3 are stable, then unstable, then stable again before they disappear.

So the damping coefficient values exist for which the eigenvalues produce the conditions for Hopf bifurcation.

Although the motor is an electromechanical device, we easily notice that the occurrence of Hopf bifurcation is conditioned by a special relationship between two electrical parameters. Equation (24) also shows the combined impact of the mechanical ratio b/J and the electrical damping ratio R/L.

4 Illustration and discussion

We now illustrate the bifurcation with the damping coefficient as the bifurcation parameter. Given the parameters

$$k_t = 0.031 \text{ N} \cdot \text{m/A}, \ n = 4, \ L = 14.25 \times 10^{-3} \text{ H},$$
$$R = 0.9 \ \Omega, \ J = 4.7 \times 10^{-5} \text{ kgm}^2,$$

when $v_d = -27$ V we have $b_{H1} = 0.007758974260878$ and $b_{H2} = 0.014528633351044$ while $b_{H0} = -0.034161291822448$. For these two positive points b_{H1} and b_{H2} in Eq. (11), we apply the center manifold theorem and normal form theory and obtain non-zero first Lyapunov coefficients at both values. We have supercritical Hopf bifur-

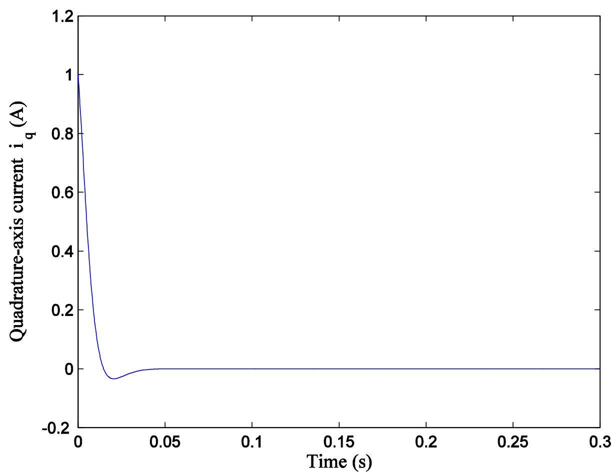

(a) Time series for $v_d \geq -k_t R/L$

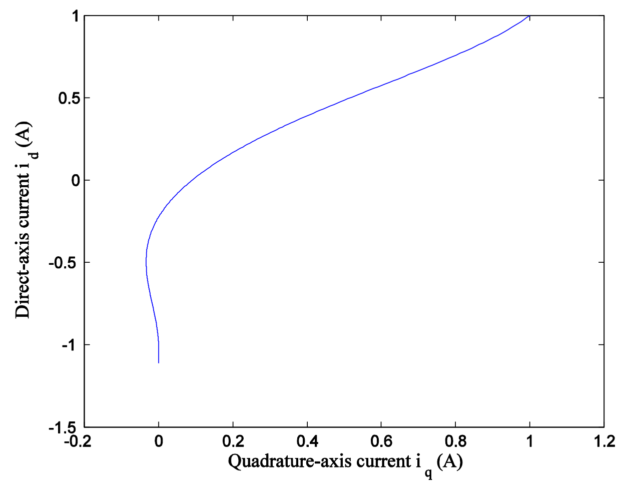

(b) Phase trajectory for $v_d \geq -k_t R/L$

Fig. 9 Another special case

cation at both points. Equilibria E_2 and E_3 are stable, then unstable, then stable again before they disappear. In Fig. 1a, the equilibrium E_1 is unstable (in cyan color) and stable (in black). Then equilibrium E_2 is unstable (in red) and stable (in magenta). And finally, equilibrium E_3 is unstable (in blue) and stable (in green color).

Chaos exists only between the two critical values b_{H1} [Eq. (11b)] and b_{H2} [Eq. (11c)] as shown as Fig. 1a, b, where $(L_1, L_2, L_3) = (+, 0, -)$. Both symmetric equilibria are saddle fulfilling the Shilnikov condition. Beyond that region, the symmetric equilibria are still saddle, but they do not satisfy the Shilnikov theorem.

We illustrate below the different scenario with the different critical values.

4.1 Case of the first bifurcation point

The system has the first Hopf bifurcation at b_{H1} [Eq. (11b)]. Around the equilibria E_2 and E_3, the limit cycle is observed, as illustrated in Fig. 2. Far from E_2 and E_3, it has the non-Shilnikov self-excited chaos (Fig. 3).

4.2 Case between two Hopf bifurcation points

Then, consider the value between b_{H1} and b_{H2}. We observe the Shilnikov self-excited chaos even when starting from the symmetrical equilibria, as shown in Fig. 4. The trajectory starts almost as stable, then starts oscillating almost periodically and then ends chaotic, which is the opposite for scenarios with transient chaos.

4.3 Case for the second Hopf bifurcation point

At b_{H2} [Eq. (11c)] the BLDCM exhibits a limit cycle near equilibria in Fig. 5 and non-Shilnikov self-excited chaos far from the equilibria (Fig. 6). Coexistence of different dynamical behaviors is experimented. The family of limit cycles to illustrate the Hopf bifurcation is also illustrated in 3D (Fig. 7).

4.4 Exceptional case when inductance and moment of inertia are equal

Exceptions for the condition of Hopf bifurcation are also tested. For example, when $J = L$, the Hopf bifurcation does not occur, as illustrated in Fig. 8. This case is fundamental in the analogy relationship between electromechanical quantities and mechanical quantities. Inductance and moment of inertia are equivalent when electrical quantities are related to mechanical rotational quantities.

4.5 Exceptional case when bifurcation parameter is more than a certain margin

Illustratively in Fig. 9, when $v_d \geq -k_t R/L$ [Eq. (14a)], we have the only equilibrium as predicted.

4.6 Case for a single bifurcation point

For the critical value conditions $v_d = v_{d2}$ [Eq. (14b)], the BLDCM has a point where there is only one bifurcation value for the damping coefficient. Around the value, we find transient chaos, as is illustrated in Fig. 10, which depicts the change in the transient time as there are slight changes around the critical value $v_d = v_{d2}$. When $v_d = v_{d2}$, we observe Hopf bifurcation and coexistence of the limit cycle (Fig. 10e, f) and

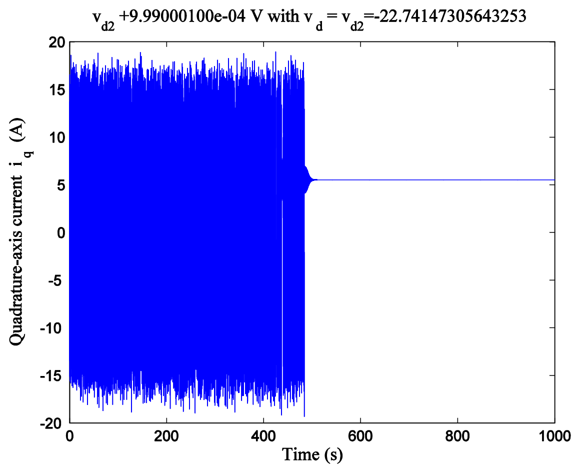

(a) Time series around $v_d = v_{d2}$

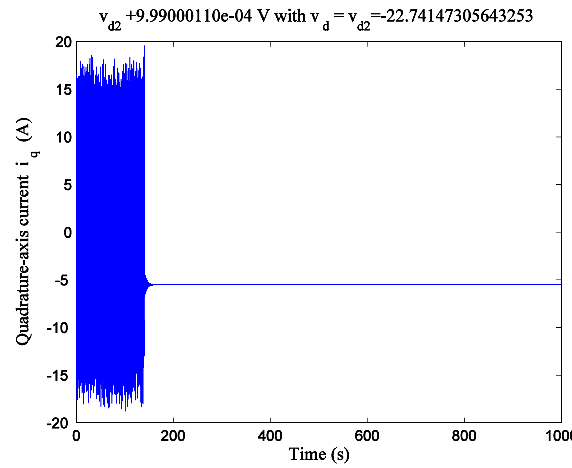

(b) Time series around $v_d = v_{d2}$

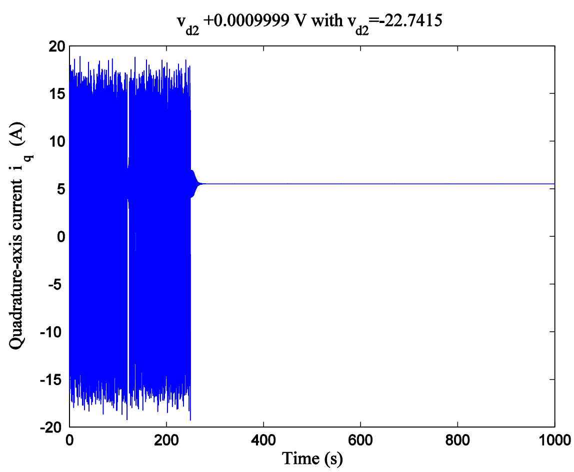

(c) Time series around $v_d = v_{d2}$

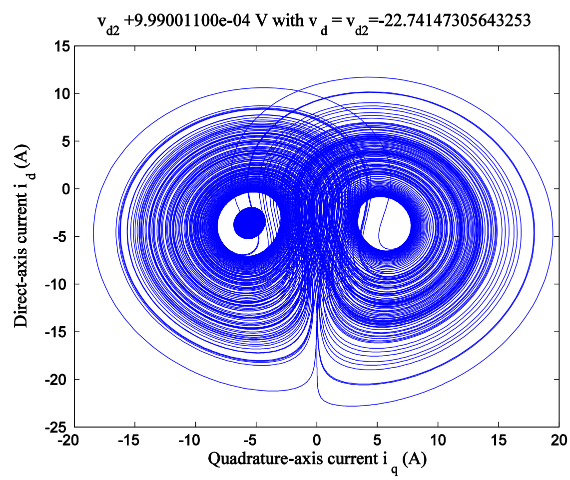

(d) Phase trajectory around $v_d = v_{d2}$

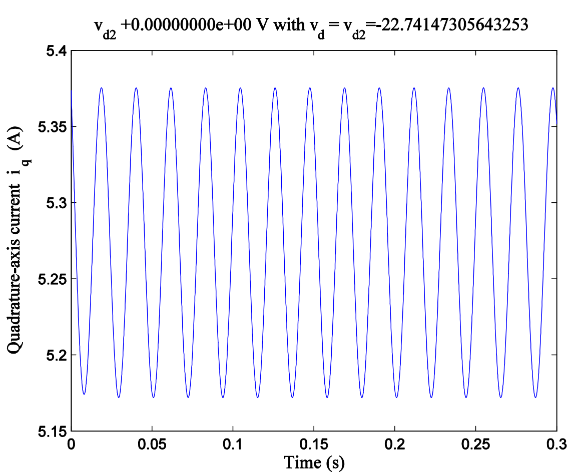

(e)Time series of the limit cycle at $v_d = v_{d2}$

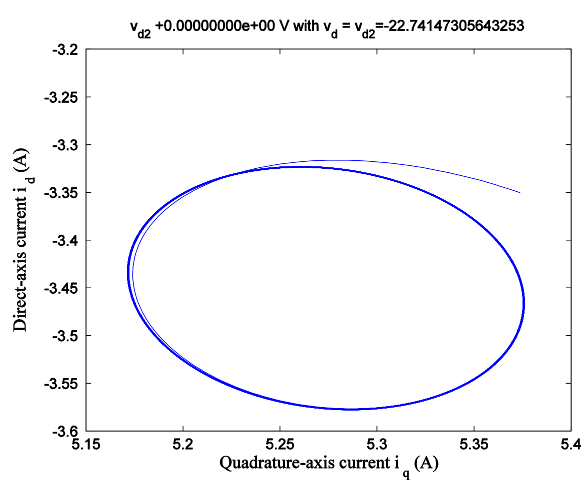

(f)Phase trajectory of the limit cycle at $v_d = v_{d2}$

Fig. 10 Particular case $v_d = v_{d2}$

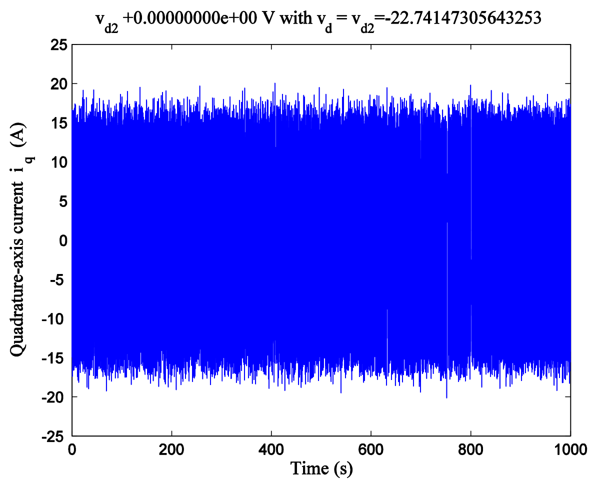

(g)Time series of chaos at $v_d = v_{d2}$

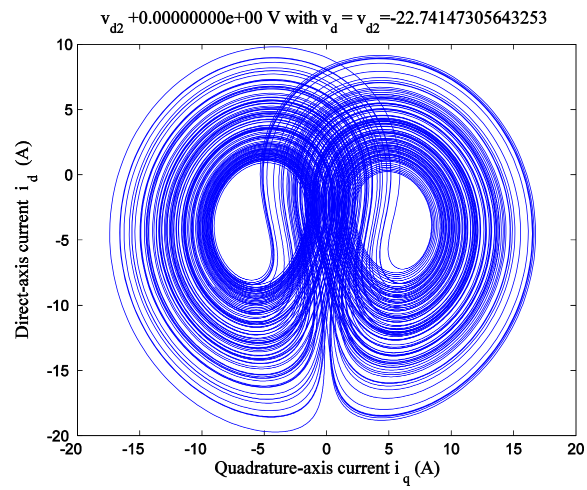

(h)Phase trajectory of chaos at $v_d = v_{d2}$

Fig. 10 continued

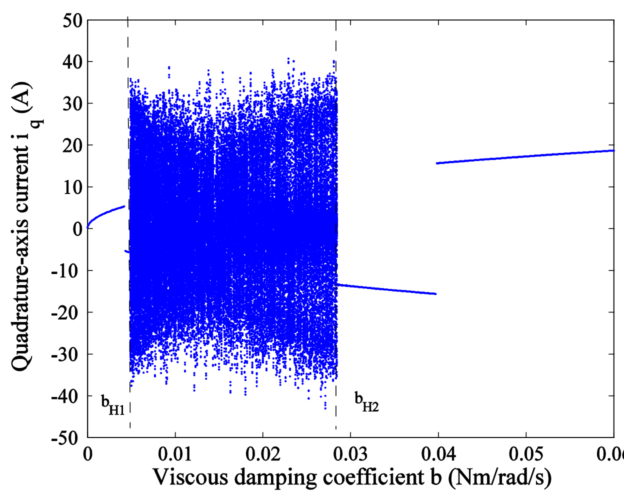

Fig. 11 Evolutionary bifurcation diagram

chaos (Fig. 10g, h). There are so many dynamical behaviors around this point because it is an exceptional point whereby two Hopf bifurcation points are combined into a single bifurcation point.

From Eq. (3), by fixing v_d, pitchfork bifurcation happens if $b = b_p$ when $b_p = -\left(n^2 L k_t v_d + R n^2 k_t^2\right) / R^2$. Three equilibrium points exist when $b < b_p$. With $v_d = -50$ V, $b_p = 0.4192$ N · m/rad/s, $b_{H1} = 0.005$ N · m/rad/s and $b_{H2} = 0.028$ N · m/rad/s. There are also two switching points, excepted to be homoclinic bifurcation points, depicting switching between symmetric equilibria.

Moreover, comparatively b_{H1} and b_{H2} (Figs. 11 and 12a), the evolutionary bifurcation diagram and the evolutionary graph of the Lyapunov exponents are similar.

Figure 12b is the reduced range of the viscous damping coefficients b values from Fig. 12a. There exist points $b_{H1} = 0.005$ N · m/rad/s and $b_{H2} = 0.028$ N · m/rad/s where the maximum $L_1 = 0$, the other two LEs are negative. This condition gives rise to limit cycles. Chaos exists in the range between $b_{H1} = 0.005$ N · m/rad/s and $b_{H2} = 0.028$ N · m/rad/s.

Comparing with the bifurcation with direct-axis v oltage, it is evident that the bifurcation with the damping coefficient gives more complexity. The damping coefficient is very influential as it participates in the definition of the dissipativity of the BLDCM model.

5 Conclusion

The BLDCM model was analyzed to focus on the viscous damping coefficient, which is a mechanical design parameter. The impact of this parameter was first found in the dissipativity of the system. The pitchfork bifurcation was identified. The onset of the Hopf bifurcation proved the impact of this parameter on the complexity of the overall dynamics. This type of bifurcation occurs twice with real positive parameters. The different scenarios for dynamical behaviors were illustrated. The chaos, limit cycle and stability were checked. Besides, transient features near the single Hopf bifurcation point were observed. The observation is that when the parameter is closer to the unique Hopf point, the transient time gets longer. Evolutionary bifurcation diagrams and Lyapunov exponents support the theoretical results that were found from rigorous methods.

This study also may suggest that parameters that define dissipativity of a system can have a greater impact on the

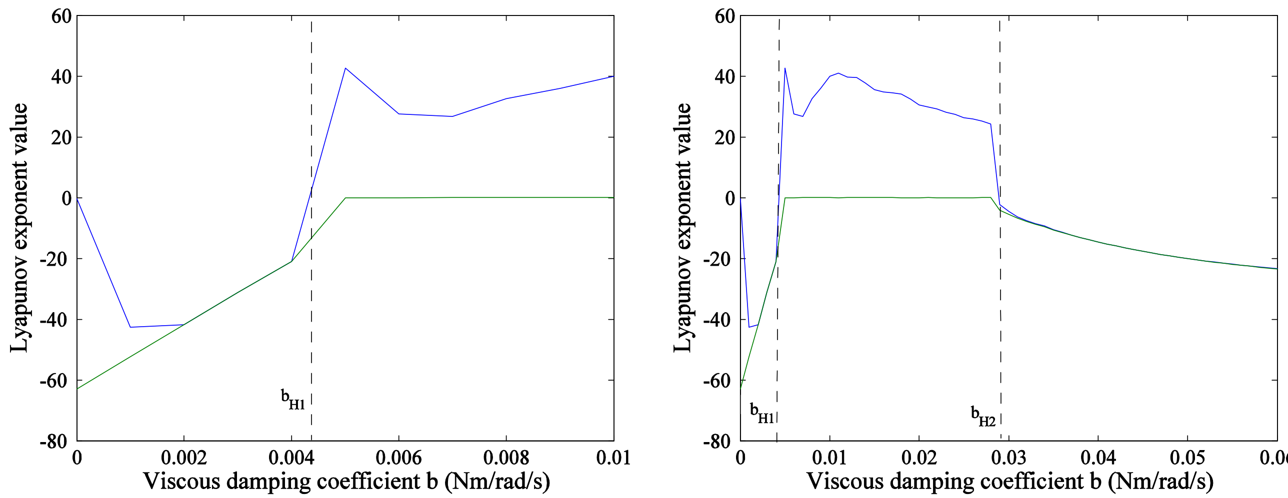

(a) Longer range of *b* (b) Smaller range of *b*

Fig. 12 Variation of Lyapunov exponents with the viscous damping coefficient

overall dynamics than a parameter that does not contribute to the dissipativity.

Acknowledgements This work was supported by the National Natural Science Foundation of China under Grant 61873186.

Authors' contributions All authors whose names appear on the submission revised it critically for important intellectual content and approved the version to be published; First author made substantial contributions to the conception or design of the work; or the acquisition, analysis, or interpretation of data; or the creation of new software used in the work;

Funding No funding was received to assist with the preparation of this manuscript.

Data availability None.

Code availability The codes used during the current study are available from the corresponding author on reasonable request.

Declarations

Conflict of interest The authors declare no conflict of interest.

References

1. Wei Z, Moroz I, Sprott JC, Akgul A, Zhang W (2017) Hidden hyperchaos and electronic circuit application in a 5D self-exciting homopolar disc dynamo. Chaos 27:033101. 4977417
2. Shinbrot T, Grebogi C, Wisdom J, Yorke JA (1992) Chaos in a double pendulum. Am J Phys 60(6):491–499. 16860
3. Zhu Q, Ishitobi M (1999) Experimental study of chaos in a driven triple pendulum. J Sound Vib 227(1):230–238
4. Faradja P, Qi G, M Tatchum M (2014) Sliding mode control of a rotary inverted pendulum using higher order differential observer. In: Proceedings of 14th international conference on control, automation and systems (ICCAS), pp 1123–1127. 6987548
5. Kitio Kwuimy CA, Woafo P (2008) Dynamics, chaos and synchronization of self-sustained electromechanical systems with clamped-free flexible arm. Nonlinear Dyn 53:201–213. 0
6. Montava Belda MA (2009) A route to chaos in electromechanical systems: phase space attraction basin switching. Int J Bifurc Chaos 19(7):2363–2375. S021812740902413X
7. Hemati N (1993) Dynamic analysis of brushless motors based on compact representations of the equations of motions. In: Proceedings of 28th IEEE industry applications conference, pp 51–58. 298903
8. Gao YM, Chau KT (2004) Hopf bifurcation and chaos in synchronous reluctance motor drives. IEEE Trans Energy Convers 19:296–302. 827012
9. Hemati N (1994) Strange attractors in brushless DC motors. IEEE Trans Circuits Syst I 41:40–45. 260218
10. Li Z, Park JB, Joo YH, Zhang B, Chen G (2002) Bifurcations and chaos in a permanent-magnet synchronous motor. IEEE Trans Circuits Syst I 49:383–387. 989176
11. Wei D, Wan L, Luo X, Zeng S, Zhang B (2014) Global exponential stabilization for chaotic brushless DC motors with a single input. Nonlinear Dyn 77(1):209–212. 0142331218802355
12. Roy P, Ray S, Bhattachary S (2015) Control of chaos in BLDC motor using modified feedback method. In: Proceedings of Michael Faraday IET international summit, pp 84–88. 1611
13. Luo S, Wang J, Wu S, Xiao K (2014) Chaos RBF dynamics surface control of brushless DC motor with time delay based on tangent barrier Lyapunov function. Nonlinear Dyn 78(2):1193–1204. x
14. Liu Z, Chen Y, Wu X (2009) Global chaos synchronization of the brushless DC motor systems via variable substitution control. In: Proceedings of 2009 international workshop on chaos-fractals theories and applications, pp 21–24
15. Ge Z, Cheng J, Chen Y (2014) Chaos anticontrol and synchronization of three time scales brushless DC motor system. Chaos Solitons Fract 22:1165–1182
16. Ge Z, Cheng J (2005) Chaos synchronization and parameter identification of three time scales brushless DC motor system. Chaos Solitons Fract 24:597–616. 031

17. Xue W, Li Y, Cang S, Jia H, Wang Z (2015) Chaotic behavior and circuit implementation of a fractional-order permanent magnet synchronous motor model. J Frankl Inst. 025
18. Lu J, Hou X (2014) Hopf bifurcation controller parameterization for a brushless DC motor system. In: Proceeding of the 11th world congress on intelligent control and automation, pp 4154–4158
19. Jabli N, Khammari H, Mimouni MF, Dhifaoui R (2010) Bifurcation and chaos phenomena appearing in induction motor under variation of PI controller parameters. WSEAS Trans Syst 9:784–793
20. Faradja P, Qi G (2018) Energy bifurcation and energy patterns of the BLDCM systems manifolds in the hidden chaos mode. In: Proceedings of 11th international workshop on chaos-fractals theories and applications (IWCFTA), p 8
21. Faradja P, Qi G (2020) Analysis of multistability, hidden chaos and transient chaos in brushless DC motor. Chaos Solitons Fract 132:109606. 109606
22. Yang Y, Qi G, Hu J, Faradja P (2020) Finding method and analysis of hidden chaotic attractors for plasma chaotic system from physical and mechanistic perspectives. Int J Bifurc Chaos 30(05):2050072. S0218127420500728
23. Bi H, Qi G, Hu J, Faradja P, Chen G (2020) Hidden and transient chaotic attractors in the attitude system of quadrotor unmanned aerial vehicle. Chaos Solitons Fract 138:109815. 109815
24. Qi G (2017) Energy cycle of brushless DC motor chaotic system. Appl Math Model 51:686–697. 025
25. Faradja P, Qi G (2020) Hamiltonian-based energy analysis for brushless DC motor chaotic system. Int J Bifurc Chaos 30(08):2050112. S0218127420501126
26. Gao Y (2005) Chaoization of PM synchronous motor drives via time-delay feedback. Doctoral thesis, University of Hong Kong
27. Faradja P, Qi G (2019) Local bifurcation analysis of brushless DC motor. Int Trans Electr Energy Syst. 2710
28. Singh JP, Roy BK, Kuznetsov NV (2019) Multistability and hidden attractors in the dynamics of permanent magnet synchronous motor. Int J Bifurc Chaos 29(4):1950056. S0218127419500561
29. Pravin JM (2000) When are the roots of a cubic real? Resonance 5(5):86–89. BF02834676